INTERNATIONAL JOURNAL FOR NUMERICAL METHODS IN FLUIDS
Int. J. Numer. Meth. Fluids 2002; **39**:141–159 (DOI: 10.1002/fld.261)

Convergence acceleration by self-adjusted time stepsize using Bi-CGSTAB method for turbulent separated flow computation

W. B. Tsai[1], W. W. Lin[2] and C. C. Chieng[3,*,†]

[1]*Department of Management Information System, Far East College, Hsin-Shih, Taiwan*
[2]*Department of Mathematics, National Tsing-Hua University, Hsinchu, Taiwan*
[3]*Department of Engineering and System Science, National Tsing-Hua University, Hsinchu, Taiwan*

SUMMARY

Poor convergence behavior is usually encountered when numerical computations on turbulent separated flow are performed. A design of self-adjusted stepsize concept both in time span and spatial coordinate systems to achieve faster convergence is demonstrated in this study. The determination of the time stepsize based on the concept of minimization of residuals using the Bi-CGSTAB algorithm is proposed. The numerical results show that the time stepsize adjusted by the proposed method indeed improves the convergence rate for turbulent separated flow computations using advanced turbulence models in low-Reynolds number forms. Copyright © 2002 John Wiley & Sons, Ltd.

KEY WORDS: convergence acceleration; self-adjusted time stepsize; Bi-CGSTAB method; turbulent separated flow

1. INTRODUCTION

The solution of the Navier–Stokes equations with higher order turbulence closure models is of fundamental importance for a wide variety of flows, turbulent separated flows in particular. However, good convergence behavior for the system of these equations is difficult to achieve. Slow convergence for such matrix systems has been greatly improved by using the conjugate gradient-series methods, such as the classical conjugate gradient method [1], the generalized conjugate gradient method (GCG) [2], the bi-conjugate gradient (Bi-CG) method [3], the conjugate gradient squared (CG-S) method [4] and the Bi-CGSTAB method [5]. The conjugate gradient method is one of the most famous iterative methods for solving the matrix system which is symmetric and positive definite. However, for general applications, the matrix systems are seldom symmetric or positive definite. The generalized conjugate gradient (GCG) method is developed based on the residual minimization for non-symmetric matrix systems, but the

*Correspondence to: Ching-Chang Chieng, Department of Engineering & Systems Science, National Tsing Hua University, 101 Section 2, Kuang Fu Road, Hsinchu, Taiwan, Republic of China.
†E-mail: cchieng@mk.nthu.edu.tw

Received 8 June 2000
Revised 19 July 2001

disadvantages of the GCG method are the possibility of breaking down and usually many search directions should be stored. The Bi-CG method solves an enlarged linear system with only one search direction, but encounters cumbersome programming as performing the product of the transpose of the coefficient matrix with a vector. Furthermore, the minimization property of the residual norm no longer exists. In the CGS method, a bilinear form is introduced and performed in the Bi-CG method and the operation of the transpose of the matrix with a vector disappears. Furthermore, it is not necessary to solve enlarged systems so the computation work of the CGS method is not greater than that of the Bi-CG method. Although the CGS method has been proposed as an attractive variant of the Bi-CG method, it has been observed that the CGS method may lead to a rather irregular convergence behavior, especially by starting the iteration close to the solution. The Bi-CGSTAB method is an extension of the CGS method, however, a more smoothing convergence behavior than CGS method is achieved since the Bi-CGSTAB method produces much more accurate residual vectors (and, hence, more accurate solutions). Moreover, the Bi-CGSTAB method is applied to accelerate the convergence rate of solving the matrix system resulting from Navier–Stokes equations, and is successful to some degree [6, 7], but the convergence rate needs further acceleration. This work proposes the additional inclusion of unsteady flow calculation, i.e. employing the time marching technique to approach steady state flow solution. For the unsteady flow computation, the decreasing of the time stepsize stablizes the convergence but increases the number of time steps to reach steady state flow condition. It implies that the choice of the time stepsize is a key issue in optimizing the computation time.

Usually, the stability analysis only provides the constraint of time stepsize for linearlized systems, but suggests no best value of the time stepsize [8, 9]. In most cases, very rough estimations plus experience can provide the guide of the selection of time stepsize for simple flows, but the guide is difficult for complex separated flows. Besides, uniform time stepsize is commonly applied for all the computational grid nodes/control volumes, except the applications of the local-time-step concept [10], which may not be feasible for complex flows.

For the local-time-step approach, the magnitude of the time stepsize depends on the cell volume of the computational cell, i.e. smaller time stepsize adopted for smaller control volume. The applications of the local-time-step method in CFD achieve some degree of improvement, for example, Saxena and Ravi [11] computed the 3-D supersonic and hyperbolic blunt body flows with TVD scheme, Arnone *et al.* [12] performed the multigrid computation of unsteady rotor–stator intersection. Mark *et al.* [13] computed a compressible flow and heat transfer in a smooth U-duct with and without rotation using second order accurate Roe's scheme and three-level V-cycle multigrid, and Soulis *et al.* [14] applied the third-order accurate flux difference upwind scheme to compute incompressible turbulent flow in turbomachinery.

The proposed method adopted the concept from the Bi-CGSTAB method [5] which is a fast and smooth convergent variant of the Bi-CG method [3], moreover, the Bi-CGSTAB method updated the solution vectors such that the two-norm minimization of the residual vectors can be obtained, thus the disadvantage of the very irregular convergence behavior by the CGS method can be avoided. Along the same lines, we extended the derivation of the Bi-CGSTAB method to unsteady state flow so that the time stepsize of the computation cell at a specific iteration step can be obtained to enforce the residual of the conservative properties of the computational cell to a minimum value, say zero.

The proposed method has been proved successful in accelerating the convergence rate by varying time stepsize for predicting the turbulent pipe flow [15]. The present study intends

to demonstrate the performance of this numerical scheme for turbulent separated flow. Two tested cases are: (1) the turbulent flow past a 2-D surface-mounted rib with a prescribed inlet velocity profile [16, 17] and (2) the periodic turbulent flow past a 2-D mounted rib with a Reynolds number of 12 600 [18]. The advanced turbulence models of Launder–Sharma [19], Chien [20], Lin and Hwang [21] and Durbin [22] are the applied models with different degrees of complexity for illustrating the improvement in convergence rate.

2. GOVERNING EQUATIONS

Turbulent flow computations solve time dependent, Reynolds averaged, incompressible Navier–Stokes equations and transport equations of turbulent properties. The governing equations in Cartesian tensor notation can be written as follows:
Continuity Equation:

$$\frac{\partial U_i}{\partial x_j} = 0 \tag{1}$$

Momentum Equations:

$$\frac{\partial(\rho U_i)}{\partial t} + \frac{\partial \rho U_i U_j}{\partial x_j} = -\frac{\partial P}{\partial x_j} + \frac{\partial}{\partial x_j}\left[\mu\left(\frac{\partial U_i}{\partial x_j} + \frac{\partial U_j}{\partial x_i}\right) - \rho\overline{u_i u_j}\right] \tag{2}$$

where U_i is the velocity in the x_i direction, P represents the pressure, μ is the molecular viscosity and the Reynolds stress $\rho\overline{u_i u_j}$ can be approximated by adopting Boussinesq approximation within the framework of eddy viscosity, i.e.

$$-\rho\overline{u_i u_j} = \mu_t\left(\frac{\partial U_i}{\partial x_j} + \frac{\partial U_j}{\partial x_i}\right) - \frac{2}{3}\delta_{ij}k \tag{3}$$

and μ_t is the turbulent viscosity, δ_{ij} is the delta function, and k is the turbulent kinetic energy. Turbulent properties $-\rho\bar{u}_i\bar{u}_j$ or μ_t are solved by turbulence models described in following paragraphs.

2.1. Turbulence property equations in low-reynolds number form

The turbulent properties can be obtained by transport equations and the formulations of turbulent kinetic energy (k) and its dissipation rate (ε) by various turbulence models are briefly stated as follows:

- $k-\varepsilon$ model

$$\frac{\partial(\rho k)}{\partial t} + \frac{\partial(\rho U_j k)}{\partial x_j} = \frac{\partial}{\partial x_j}\left[\left(\mu + \frac{\mu_t}{\sigma_k}\right)\frac{\partial k}{\partial x_j}\right] - \rho\overline{u_i u_j}\frac{\partial U_i}{\partial x_j} - \rho(\bar{\varepsilon} + D) \tag{4}$$

$$\frac{\partial(\rho\bar{\varepsilon})}{\partial t} + \frac{\partial(\rho U_j\bar{\varepsilon})}{\partial x_j} = \frac{\partial}{\partial x_j}\left[\left(\mu + \frac{\mu_t}{\sigma_\varepsilon}\right)\frac{\partial\bar{\varepsilon}}{\partial x_j}\right] - \rho C_{\bar{\varepsilon}1} f_1 \frac{\bar{\varepsilon}}{k}\overline{u_i u_j}\frac{\partial U_i}{\partial x_j} - \rho C_{\bar{\varepsilon}2} f_2 \frac{\bar{\varepsilon}^2}{k} + E \tag{5}$$

$$\mu_t = \rho C_\mu f_\mu \frac{k^2}{\bar{\varepsilon}}, \quad \varepsilon = \bar{\varepsilon} + D \tag{6}$$

Table I. Constants and damping functions for the Launder–Sharma model (LS) and Chien model (CH).

	LS	CH
C_μ	0.09	0.09
f_μ	$\exp\left(-\frac{3.4}{(1+0.02R_t)^2}\right)$	$1-\exp(-0.0115y^+)$
σ_k	1.0	1.0
$\sigma_{\tilde{\varepsilon}}$	1.3	1.3
D	$2\upsilon\left(\frac{\partial\sqrt{k}}{\partial y}\right)^2$	$2\upsilon\frac{k}{y^2}$
E	$2\upsilon\upsilon_1\left(\frac{\partial^2 U_i}{\partial x_j\partial x_k}\right)^2$	$-2\upsilon\left(\frac{\tilde{\varepsilon}}{y^2}\right)\exp(-0.5y^*)$
f_1	1	1
f_2	$1-0.3\exp(-R_t^2)$	$1-0.22\cdot\exp\left(-\frac{R_t^2}{36}\right)$
$C_{\tilde{\varepsilon}1}$	1.44	1.35
$C_{\tilde{\varepsilon}2}$	1.92	1.8
R_t	$\frac{k^2}{\upsilon\tilde{\varepsilon}}$	$\frac{k^2}{\upsilon\tilde{\varepsilon}}$
y^+		$\frac{yU_\tau}{\upsilon}$

The constants and damping functions for the models of Launder–Sharma (LS) [19] and Chien (CH) [20] in the above equations are listed in Table I.

- Lin's $k-\tilde{\varepsilon}$ model [21]

$$\frac{\partial(\rho k)}{\partial t}+\frac{\partial(\rho U_j k)}{\partial x_j}=\frac{\partial}{\partial x_j}\left[\left(\mu+\frac{\mu_t}{\sigma_k}\right)\frac{\partial k}{\partial x_j}\right]+\prod_k-\rho\overline{u_iu_j}\frac{\partial U_i}{\partial x_j}-\rho(\tilde{\varepsilon}+\hat{\varepsilon}) \tag{7}$$

$$\frac{\partial(\rho\tilde{\varepsilon})}{\partial t}+\frac{\partial(\rho U_j\tilde{\varepsilon})}{\partial x_j}=\frac{\partial}{\partial x_j}\left[\left(\mu+\frac{\mu_t}{\sigma_\varepsilon}\right)\frac{\partial\tilde{\varepsilon}}{\partial x_j}\right]+\prod_{\tilde{\varepsilon}}-\rho C_{\tilde{\varepsilon}}f_1\frac{\tilde{\varepsilon}}{k}\overline{u_i}\,\overline{u_j}\frac{\partial U_i}{\partial x_j}-\rho C_{\tilde{\varepsilon}2}f_2\frac{\tilde{\varepsilon}^2}{k} \tag{8}$$

$$\mu_t=\rho C_\mu f_\mu\frac{k^2}{\tilde{\varepsilon}},\quad \varepsilon=\tilde{\varepsilon}+\hat{\varepsilon} \tag{9}$$

and the constants and damping functions for Lin's models in the above equations are listed in Table II.

Table II. Constants and damping functions for Lin's $k-\tilde{\varepsilon}$ model.

Lin's $k-\tilde{\varepsilon}$ Model	
C_μ	0.09
σ_k	$1.4-1.1\cdot\exp\left(-\frac{y_\lambda}{10}\right)$
$\sigma_{\tilde{\varepsilon}}$	$1.3-\exp\left(-\frac{y_\lambda}{10}\right)$
$C_{\tilde{\varepsilon}1}$	1.44
$C_{\tilde{\varepsilon}2}$	1.92
y_λ	$\frac{y\sqrt{\tilde{\varepsilon}}}{\sqrt{\upsilon k}}$
f_μ	$1-\exp\left(-\frac{y_\lambda}{100}-\frac{8y_\lambda^3}{1000}\right)$
$\prod_k$	$-\frac{1}{2}\frac{\partial}{\partial x_j}\left(\mu\frac{k}{\varepsilon}\frac{\partial\hat{\varepsilon}}{\partial x_j}\right)$
$\prod_{\tilde{\varepsilon}}$	$-\frac{\partial}{\partial x_j}\left(\mu\frac{\tilde{\varepsilon}}{k}\frac{\partial k}{\partial x_j}\right)$
$\hat{\varepsilon}$	$2\upsilon\left(\frac{\partial\sqrt{k}}{\partial y}\right)^2$
f_1	1
f_2	$1-0.22\cdot\exp\left(-\frac{R_t^2}{36}\right)$
R_t	$\frac{k^2}{\upsilon\tilde{\varepsilon}}$

- Durbin's $k-\varepsilon-v^2$ model [22]

$$\frac{\partial(\rho k)}{\partial t}+\frac{\partial(\rho U_j k)}{\partial x_j}=\frac{\partial}{\partial x_j}\left[\left(\mu+\frac{\mu_t}{\sigma_k}\right)\frac{\partial k}{\partial x_j}\right]+P_k-\rho\varepsilon \tag{10}$$

$$\frac{\partial(\rho\varepsilon)}{\partial t}+\frac{\partial(\rho U_j\varepsilon)}{\partial x_j}=\frac{\partial}{\partial x_j}\left[\left(\mu+\frac{\mu_t}{\sigma_\varepsilon}\right)\frac{\partial\varepsilon}{\partial x_j}\right]+\frac{\rho C_{\varepsilon1}P_k-\rho C_{\varepsilon2}\varepsilon}{T} \tag{11}$$

$$\frac{\partial(\rho\overline{v^2})}{\partial t}+\frac{\partial(\rho U_j\overline{v^2})}{\partial x_j}=\frac{\partial}{\partial x_j}\left[\left(\mu+\frac{\mu_t}{\sigma_k}\right)\frac{\partial\overline{v^2}}{\partial x_j}\right]+\rho k f-\rho\overline{v^2}\frac{\varepsilon}{k} \tag{12}$$

$$L^2\nabla^2 f-f=(1-C_1)\frac{\left[\frac{2}{3}-\frac{\overline{v^2}}{k}\right]}{T}-C_2\frac{P_k}{k} \tag{13}$$

Table III. Constants and damping functions for Durbin's $k-\varepsilon-v^2$ model.

Durbin's $k-\varepsilon-v^2$ model	
σ_k	1.0
σ_ε	1.3
$C_{\varepsilon 1}$	$1.3+\dfrac{0.25}{1+(d/2\ell)^8}$
d	distance to the closest boundary
ℓ	$\dfrac{L}{C_L}$
$C_{\varepsilon 2}$	1.9
C_μ	0.19
C_L	0.3
C_η	70
C_1	1.4
C_2	0.3
L	$C_L \max\left(\dfrac{k^{1.5}}{\varepsilon}, C_\eta\left(\dfrac{\upsilon^3}{\varepsilon}\right)^{\frac{1}{4}}\right)$
T	$\max\left(\dfrac{k}{\varepsilon}, 6\left(\dfrac{\upsilon}{\varepsilon}\right)^{\frac{1}{2}}\right)$

$$\mu_t = \rho C_\mu \overline{v^2} T \tag{14}$$

The constants and damping functions for Durbin's models in the above equations are listed in Table III.

3. NUMERICAL FORMULATION

In order to discretize the governing equations, finite volume approach with staggered grid arrangements are employed. According to expressions of Patankar [23], the difference equations for every control volume can be expressed in the following form

$$\left[a_p^* + \frac{\rho\, \mathrm{vo}\ell}{\Delta t}\right]\phi_p^{k+1} = \sum a_{nb}\phi_{nb}^{k+1} + c_P^* + \frac{\rho\, \mathrm{vo}\ell}{\Delta t}\phi_p^k + S_p\phi_P^{k+1} + S_u \tag{15}$$

where a_{nb} represents the positive coefficients a_E, a_W, a_N, a_S which are obtained by a hybrid scheme for convective terms and a central difference scheme for diffusion terms, a_P^* is the sum of these neighbor coefficients, i.e. $a_P^* = a_E + a_W + a_N + a_S$; $\mathrm{vo}\ell$ represents the volume of the cell-P, Δt is the time stepsize at cell-P, ρ is the density and S_u and S_p are the source terms ($S_p \leqslant 0$). Therefore, the equations can be casted into

$$\left[a_P + \frac{\rho\,\mathrm{vo}\ell}{\Delta t}\right]\phi_p^{k+1} = \sum a_{nb}\phi_{nb}^{k+1} + c_P + \frac{\rho\,\mathrm{vo}\ell}{\Delta t}\,\phi_p^k \tag{16}$$

where $a_p = a_p^* - S_p$, $c_p = c_p^* + S_u$. The difference equations can also be represented as the following matrix form at the kth time step,

$$(A_k + D_{k+1})\phi_{k+1} = b_k + D_{k+1}\phi_k \tag{17}$$

where the vectors ϕ_k, ϕ_{k+1} represent the solutions for the kth and $(k+1)$th time step respectively, the coefficient matrix A_k is a penta-diagonal M-matrix and D_{k+1} is a positive diagonal matrix relating the stepsize, i.e. D_{k+1} is a positive diagonal matrix and the jth diagonal element is $\mathrm{diag}(D_{k+1})_j = \rho_j \cdot \mathrm{vo}\ell_j/\Delta t_j$, where ρ_j, $\mathrm{vo}\ell_j$ and Δt_j are the density, volume and time stepsize for the jth control volume respectively. Traditionally, the time stepsize Δt_j is set to be a constant, but the time stepsize of the proposed method is different for each control volume and is determined from the Bi-CGSTAB method due to the residual minimization.

4. TIME STEPSIZE DETERMINATION

It is well known that the small time stepsize will cause slow convergence but large stepsize will lead to divergence or oscillation for the numerical simulation. Usually, the time stepsize Δt has a restriction according to the stability criteria, and there is little information that can be assessed to balance faster convergence and instability [8, 9]. A suggestion on the optimal choice of the time stepsize is of interest.

Before the numerical procedure, the governing equations are transformed to difference equations as a linear system of $(A_k + D_{k+1})\phi_{k+1} = b_k + D_{k+1}\phi_k$. The coefficient matrix A_k and the right-hand-side vector b_k are computed from the kth time step solutions. Matrix D_{k+1} is a diagonal matrix and its elements are evaluated at $(k+1)$th step. The residual vector for the kth time step is defined by $r_k = b_k + A_k\phi_k + D_k(\phi_{k-1} - \phi_k)$. Compared to existing iterative algorithms solving the matrix system, an additional parameter as an adjustable time stepsize from the analogy of the iterative method of the Bi-CGSTAB [3] algorithm is derived and described as follows.

Table IV lists two solution procedures of two iterative algorithms to solve $Ax = b$ and $(A_k + D_{k+1})\phi_{k+1} = b_k + D_{k+1}\phi_k$, which conveys the idea determining the time stepsize. Algorithm I uses the solution procedure for the standard Bi-CGSTAB algorithm while solving a linear system of the form $Ax = b$. The initial residual $r_0 = b - Ax_0$ is defined from the initial guess x_0. According to the algorithm, the next solution vector and residual vector are $x_1 = x_0 + \alpha p_1 + \omega_1 s$ and $r_1 = s - \omega_1 t$ respectively, and the parameter ω_1 is derived from the minimization of the vector r_1. Hence, the solution vector is updated under the restriction of the two-norm minimization of the corresponding residual vector. Consequently, the $(i+1)$th approximation solution is updated from the relation $x_{i+1} = x_i + \alpha p_i + \omega_{i+1} s$, where the parameter ω_{i+1} makes the residual norm $\|r_{i+1}\|_2 = \|s - \omega_{i+1} t\|_2$ a minimal value.

Table IV. Comparison of conventional iterative Bi-CGSTAB algorithm (Algorithm I) with the proposed solution procedure (Algorithm II).

Algorithm I	Algorithm II
Solve $Ax = b$	Solve $(A_k + D_{k+1})x_{k+1} = b_k + D_{k+1}x_k$
Give x_0 and $r_0 = b - Ax_0$ Choose $\hat{r}_0 = r_0$ $\rho_0 = \alpha = \omega_0 = 1,\ v_0 = p_0 = 0$ For $i = 1, 2, 3, \ldots$ $\rho_i = (\hat{r}_0, r_{i-1})$ $\beta = \frac{\rho_i}{\rho_{i-1}}\ \frac{\alpha}{\omega_{i-1}}$ $p_i = r_{i-1} + \beta(p_{i-1} - \omega_{i-1}v_{i-1})$ $v_i = Ap_i$ $\alpha = \frac{\rho_i}{(\hat{r}_0, v_i)}$ $s = r_{i-1} - \alpha v_i$ $t = As$ $\omega_i = \frac{(t,s)}{(t,t)}$ $x_i = x_{i-1} + \alpha p_i + \omega_i s$ If x_i is accurate enough then stop $r_i = s - \omega_i t$ $i = i + 1$ endfor	Give x_0 and $r_0 = b_0 - A_0x_0$ Choose $\hat{r}_0 = r_0$ $\rho_0 = \alpha = \omega_0 = 1,\ v_0 = p_0 = 0$ For $k = 0, 1, 2, \ldots$ $\rho_{k+1} = (\hat{r}_0, r_k)$ $\beta = \frac{\rho_{k+1}}{\rho_k}\ \frac{\alpha}{\omega_k}$ $p_{k+1} = r_k + \beta(p_k - \omega_k v_k)$ $v_{k+1} = (A_k + D_k)p_{k+1}$ $\alpha = \frac{\rho_{k+1}}{(\hat{r}_0, v_{k+1})}$ $s = r_k - \alpha v_{k+1}$ $t = (A_k + D_k)s$ $\omega_{k+1} = \frac{(t,s)}{(t,t)}$ Determine D_{k+1} from $(A_k + D_{k+1})^{-1}[res\_x^k + D_k(x_k - x_{k-1})]$ $= \alpha p_{k+1} + \omega_{k+1}s$ Solve x_{k+1} from $(A_k + D_{k+1})x_{k+1} = b_k + D_{k+1}x_k$ If x_i is accurate enough then stop Compute $A_{k+1}b_{x+1}$ $res\_x^{k+1} = r_{k+1}$ $= b_{k-1} - A_{k+1}x_{k+1} + D_{k+1}(x_k - x_{k+1})$ $k = k + 1$ endfor

In the present paper, the concept of minimizing residual is extended to the time span in the computation of separated flow, such that the chosen time stepping will enforce the residual to a minimum value in the next time step. Algorithm II in Table IV is designed to determine the time stepsize for solving the linear system $(A_k + D_{k+1})\phi_{k+1} = b_k + D_{k+1}\phi_k$ in each time step, where D_{k+1} involves the stepsize Δt but A_k involves no Δt. In Algorithm II, the coefficient matrix A_0 and the vector b_0 are obtained from the initial guess x_0, and the residual vector thus can be defined as $r_0 = b_0 - A_0x_0$. Moreover, $A_k,\ x_k,\ r_k$ are the coefficient matrix, solution vector and residual vector at the kth time step respectively and the linear system

$$(A_k + D_{k+1})x_{k+1} = b_k + D_{k+1}x_k \tag{18}$$

are solved at the $(k+1)$th time step. Similar to the procedure in Algorithm I, the solution vector x_{k+1} for the $(k+1)$th time step follows both $x_{k+1} = x_k + \alpha p_{k+1} + \omega_{k+1}s$ and D_{k+1} needs to be determined such that the system of Equation (18) can be solved.

Since the residual vectors are defined by

$$r_k = b_k - A_k x_k + D_k(x_{k-1} - x_k) \tag{19}$$

and x_k is updated to x_{k+1} by

$$x_{k+1} = x_k + \alpha p_{k+1} + \omega_{k+1} s \tag{20}$$

Subtracting Equation (18) by $(A_k + D_{k+1})x_k$ on both sides of equal sign, Equation (18) yields to

$$(A_k + D_{k+1})(x_{k+1} - x_k) = b_k + D_{k+1}x_k - (A_k + D_{k+1})x_k = b_k - A_k x_k \tag{21}$$

Substituting Equation (19) to Equation (21), we have

$$(A_k + D_{k+1})(x_{k+1} - x_k) = r_k - D_k(x_{k-1} - x_k) \tag{22}$$

Combining Equations (20) and (22) we can determine D_{k+1} by the following relation

$$(A_k + D_{k+1})(\alpha p_{k+1} + \omega_{k+1} s) = r_k - D_k(x_{k-1} - x_k) \tag{23}$$

or the following relation

$$D_{k+1}(\alpha p_{k+1} + \omega_{k+1} s) = r_k - D_k(x_{k-1} - x_k) - A_k(\alpha p_{k+1} + \omega_{k+1} s) \tag{24}$$

Note that D_{k+1} is a positive diagonal matrix and $\mathrm{diag}(D_{k+1})_j = \frac{\rho_j \cdot \mathrm{vo}\ell_j}{\Delta t_j}$, where ρ_j, $\mathrm{vo}\ell_j$ and Δt_j are the density, volume and time stepsize for the jth control volume respectively. Thus the time stepsize at each control volume at a different instant of time is different, which is completely different from the conventional methods.

5. RESULTS AND DISCUSSIONS

Two separated flow cases are computed to demonstrate the performance of the concept of self-adjusted time-step: (1) the turbulent flow past a 2-D mounted rib with a prescribed inlet velocity profile [16, 17] (2) the periodic turbulent flow past a 2-D mounted rib with a Reynolds number of 12 600 [18]. In order to compare the effectiveness of the time stepsize setting, four different ways of time stepsize Δt are set, (1) Δt is set to a reasonable large number $(\Delta t)_{\max}$, (2) Δt is chosen as a reasonable small number $(\Delta t)_{\min}$, (3) Δt is adjusted by experience or trial-and-error so that a reasonably good convergence rate and characteristics can be obtained, which is denoted by $(\Delta t)_{\mathrm{const}}$, (4) Δt is adjusted according to the Bi-CGSTAB method and is confined between $(\Delta t)_{\max}$ and $(\Delta t)_{\min}$. By the concept of domain of dependence, the time stepsize $(\Delta t)_{\max}$ and $(\Delta t)_{\min}$ are evaluated conservatively as $(\Delta t)_{\max} = L/U_{\mathrm{ref}} \cdot 1/10$ and $(\Delta t)_{\min} = L/U_{\mathrm{ref}} \cdot 1/100$ respectively, where L and U_{ref} are the travel distance and the reference velocity in the axial direction respectively.

Figure 1(a) plots the convergence histories of the axial velocity by Chien's model for the test case 1. This figure compares the convergence histories by various choices of time stepsize setting. The observations are as follows. (1) The residual histories display large oscillations and lead to poor convergence performance for the time stepsize of $(\Delta t)_{\max}$. (2) If the time stepsize is reduced to a small constant time stepsize $(\Delta t)_{\min}$, the residual can be smoothly reduced to 3×10^{-5} after 1278 time steps. (3) After many tests runs, the time stepsize of $\Delta t \approx 3.1 \times (\Delta t)_{\min}$ gives us the fastest convergence rate if the time stepsize is a constant, e.g. residual is reduced to 3×10^{-5} in 815 iterations. The trial-and-error approach to choose the time stepsize is not a good approach because it is not economical. (4) The proposed concept of determining the time stepsize using the Bi-CGSTAB method and varying the stepsize at

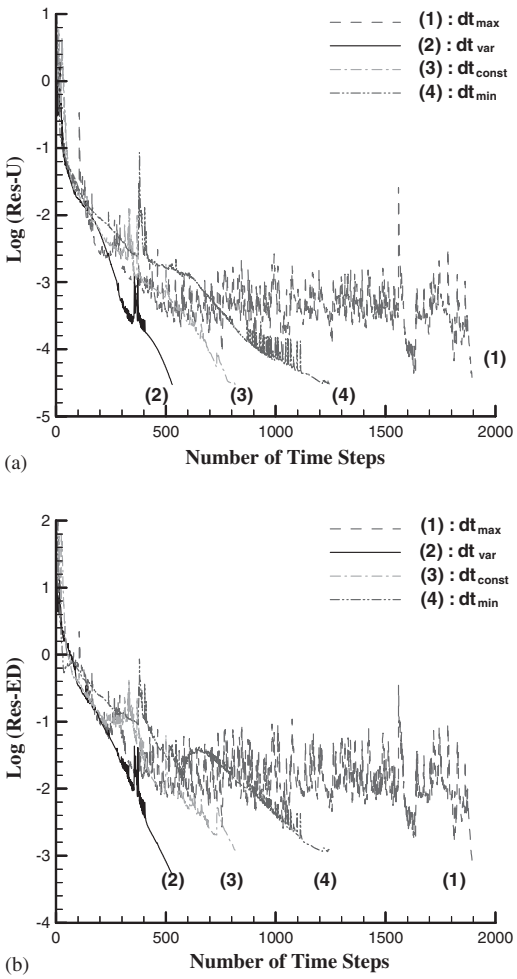

Figure 1. Residual histories for tested case 1 using Chien's model (CH). (a) Velocity U; (b) turbulent energy dissipation rate.

every cell and at every time step does give the best performance, i.e. fastest convergence rate among these four histories. Severe oscillations are observed for solving the turbulent energy dissipation equation using all strategies of time stepsize setting, but the strategy of using self-adjusted time stepsize exhibits the best rate to achieve the convergence (Figure 1(b)). Since the proposed method suggests economical time stepsize to achieve the minimum residual vector for each iteration and individual variables, converged solutions can be reached in a lower number of time steps.

Among higher order turbulence models, Chien's model is one of the models exhibiting reasonable stability and good convergence characteristic. Usually, more complex models need more experiences and special treats to achieve convergence. Three more turbulence mod-

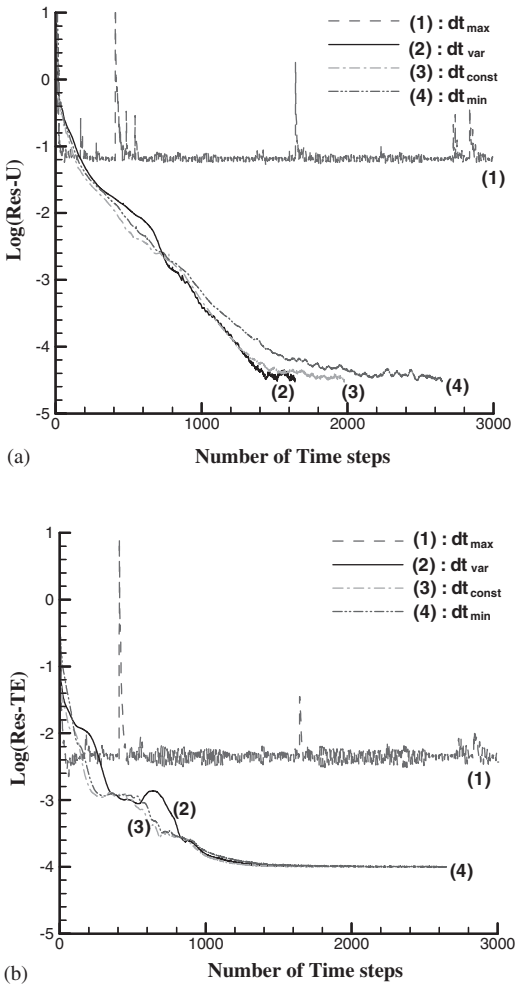

Figure 2. Residual histories for tested case 1 using Launder–Sharma's (LS) model. (a) Velocity U; (b) turbulent kinetic energy.

els are chosen to demonstrate the effectiveness of the concept of self-adjusted time stepsize: one well-known model—Launder and Sharma's—and two recently developed turbulence models—Lin's $k-\tilde{\varepsilon}$ and Durbin's $k-\varepsilon-v^2$ models. Figure 2(a) shows the convergence histories of axial velocities computed by the Launder–Sharma model. High residual levels are observed for large time stepsize $(\Delta t)_{\max}$, and the residual levels cannot be lowered to the desired criterion. Decreasing the time stepsize to a small value of $(\Delta t)_{\min}$ stabilizes the residual level and yields smooth histories; moreover, the appropriate choice of the time stepsize as $(\Delta t)_{\text{const}} \approx 2.5 \times (\Delta t)_{\min}$ can improve the convergence rate to some extent. The proposed method of varying the time stepsize using the Bi-CGSTAB algorithm can further stabilize the computation and increase the convergence rate slightly. The settings of three time stepsizes

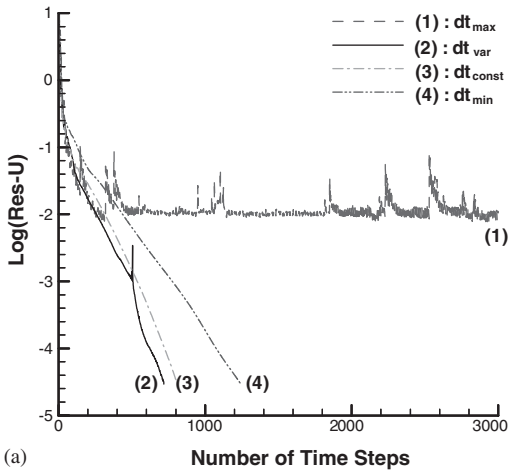

Figure 3. Residual histories for tested case 1 using Lin's model. (a) Velocity U; (b) turbulent kinetic energy.

$(\Delta t)_{\min}$, $(\Delta t)_{\text{const}} \approx 2.5 \times (\Delta t)_{\min}$ and varying time stepsize $(\Delta t)_{\text{var}}$ produce convergence performance of roughly the same degree, which implies the high degree of difficulty in achieving convergence, and small time stepsize is preferred.

More complicated terms have been introduced in Lin's model, i.e. the inclusion of the diffusive nature in the pressure diffusion term, the extra source term for ε-equation in the buffer zone, and the commonly adopted term as format $\mu\mu_t/\rho(\partial U_i/\partial x_j \partial x_k)^2$. Therefore, Lin's model not only conforms with the near wall characteristics obtained with the direct numerical simulation data but also possesses the correct asymptotic behavior in the vicinity of the wall. However, the complicated terms such as the pressure diffusion term $\prod_k$ in the k-equation and the extra term $\prod_{\tilde{\varepsilon}}$ in $\tilde{\varepsilon}$-equation cause instabilities and thus large irregularities on the convergence histories are observed if time stepsize of $(\Delta t)_{\max}$ is chosen for axial velocity

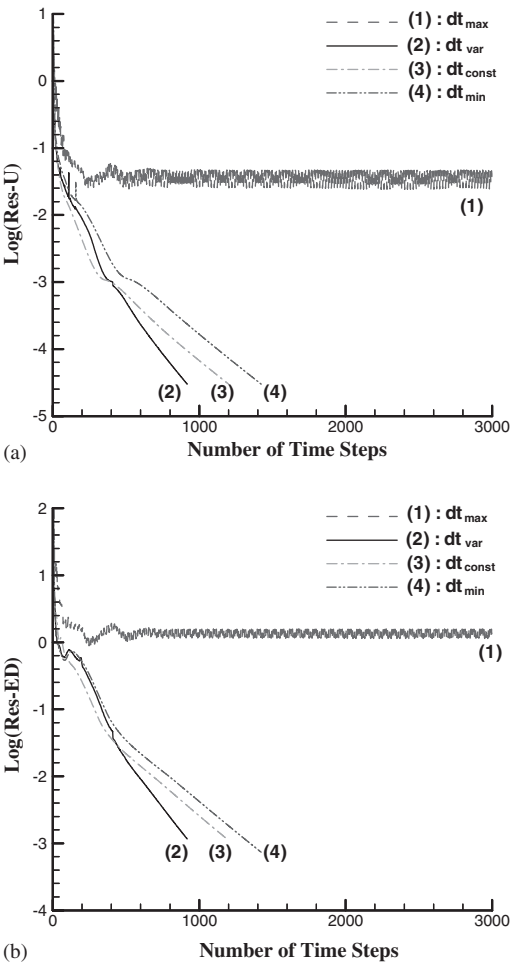

Figure 4. Residual histories for tested case 1 Durbin's $k - \varepsilon - v^2$ model. (a) Velocity U; (b) turbulent kinetic energy.

(Figure 3(a)). The adoption of self-adjusted time stepsize improves the convergence rate over the trial-and-error choice of $(\Delta t)_{\text{const}} \approx 3.1 \times (\Delta t)_{\text{min}}$ for Lin's model.

Since Durbin's model introduces additional variables $\overline{v^2}$ and f, and $\overline{v^2}$ needs to be solved via $\overline{v^2}$ transport equation and f to be solved via elliptic relaxation equations. The variable $\overline{v^2}$ is a velocity scale and might loosely be regarded as the velocity fluctuation normal to the streamlines. Also, $\overline{v^2}$ behaves as the wall normal component of turbulent intensity near the surfaces. Impermeable boundaries cause non-local suppression of $\overline{v^2}$, and the elliptic relaxation equation for f is the mathematical representation of non-locality. It is designed for use in wall-bounded flows. The difficulty of achieving convergence is obvious due to the increased number of equations. It is found that the automatic choice of the time stepsize using the

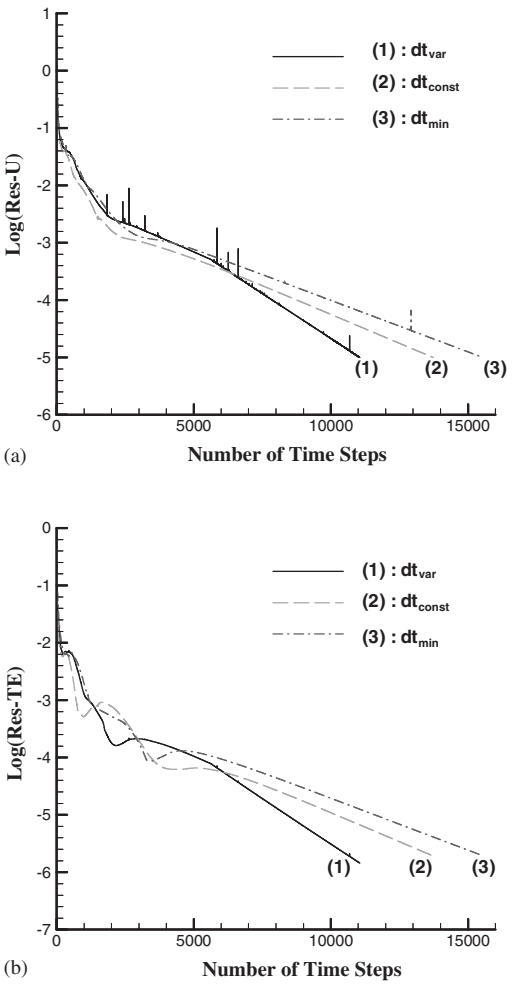

Figure 5. Residual histories for tested case 2 using Chien's (CH) model. (a) Velocity U; (b) turbulent kinetic energy.

Bi-CGSTAB algorithm indeed improves the convergence rate even more effectively for this model with a higher degree of complexity (Figure 4). Furthermore, the convergence rate for the choice of self-adjusted time stepsize lies between the rates by the choices of $(\Delta)_{\text{const}}$ and $(\Delta t)_{\min}$ for the first 400 iterations (Figures 4(a) and (b)). However, the larger time stepsize is allowed for $(\Delta t)_{\text{var}}$ setting after 400 time steps, so that the convergence is speeded up at a later stage.

From the above observations, it can be concluded that the convergence can be achieved faster by the self-adjusted time stepsize than by the pre-set time stepsize of constant values. The same conclusion can be drawn even if the advanced and complicated turbulence models are applied.

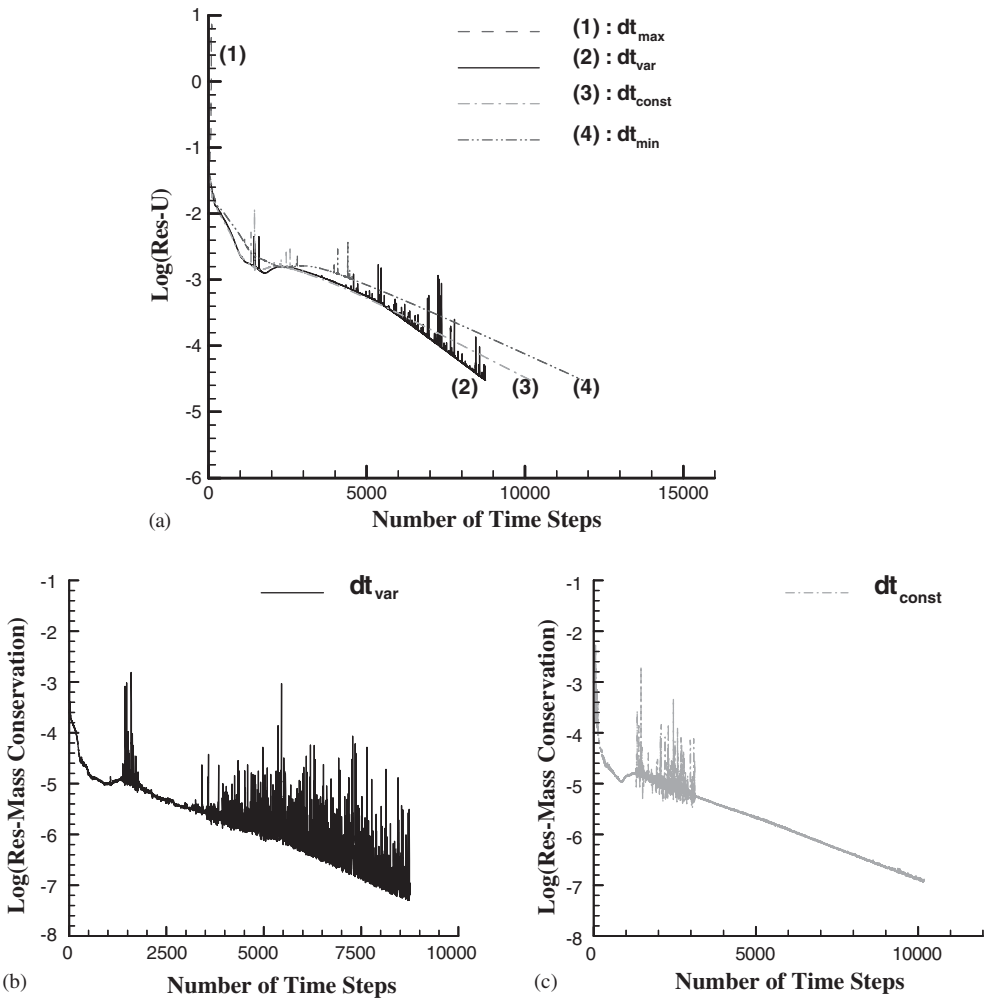

Figure 6. Residual histories for tested case 2 using Launder–Sharma's model (LS). (a) Velocity U; (b) mass-conservation ($(\Delta t)_{\text{var}}$) and (c) mass-conservation ($(\Delta t)_{\text{const}}$).

As we move on to test case 2, the computation on periodic turbulent flow past a 2-D mounted rib is performed. The convergence rate of this case is much slower than that of case 1 due to the complexity of flow-field with finer grid. Figure 5 plots the convergence histories by Chien's model for test case 2. In this figure, the convergence histories for the stepsize of $(\Delta t)_{\max}$ are not shown because it diverges within 200 iterations. The grid size in test case 2 is finer than that in test case 1 due to the requirement of y^+ less than 0.1 for the first grid next to the wall. The convergence is much more difficult to achieve and more iteration time steps are needed to obtain the converged flow-field and temperature field. In this case, the choice of self-adjusted time stepsize provides the fastest convergence rate among the settings of $(\Delta t)_{\min}$, $(\Delta t)_{\text{const}} = 3.2 \times (\Delta t)_{\min}$, and $(\Delta t)_{\text{var}}$. Figure 6 presents the

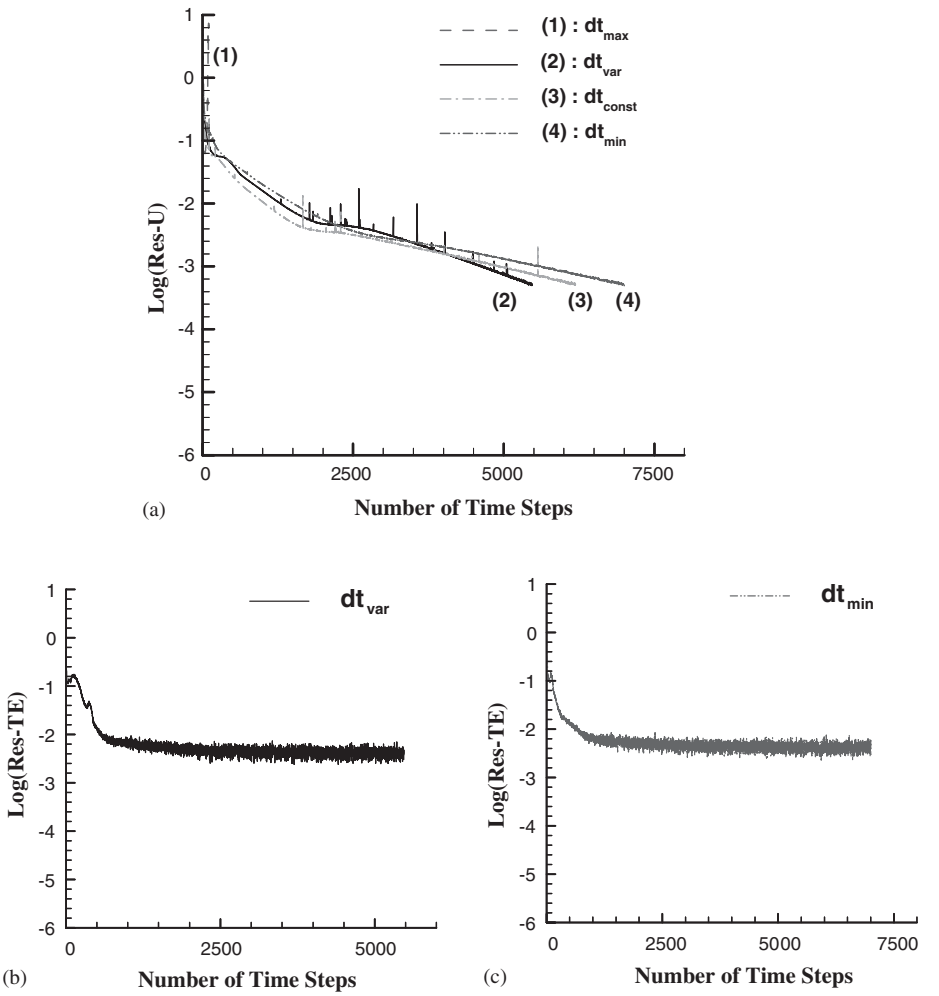

Figure 7. Residual histories for tested case 2 using Lin's model. (a) Velocity U; (b) turbulent kinetic energy ($(\Delta t)_{\text{var}}$); and (c) turbulent kinetic energy ($(\Delta t)_{\text{min}}$).

residual histories using Launder and Sharma's model. Severe oscillations for residual of mass-conservation can be found in Figure 6(b) and no oscillations are observed if the settings of the time stepsize are $(\Delta t)_{\text{const}}$ after 3500 iterations (Figure 6(c)). The self-adjusted method still provides the fastest convergence rate than the other settings of fixed time stepsize do, but the oscillations appear in the computation of axial velocity. Moreover, this figure also suggests that the spikes can be reduced if the time stepsize is set to a smaller one. Lin's model introduces a higher degree of instability so that irregularities on the convergence histories are observed for axial velocity computation in Figure 7(a). For the computation of turbulent kinetic energy, the residuals cannot be lowered down to the desired level for all settings of time stepsize, $(\Delta t)_{\text{var}}$ (Figure 7(b)) or $(\Delta t)_{\text{max}}$ (Figure 7(c)). Least improvement is achieved

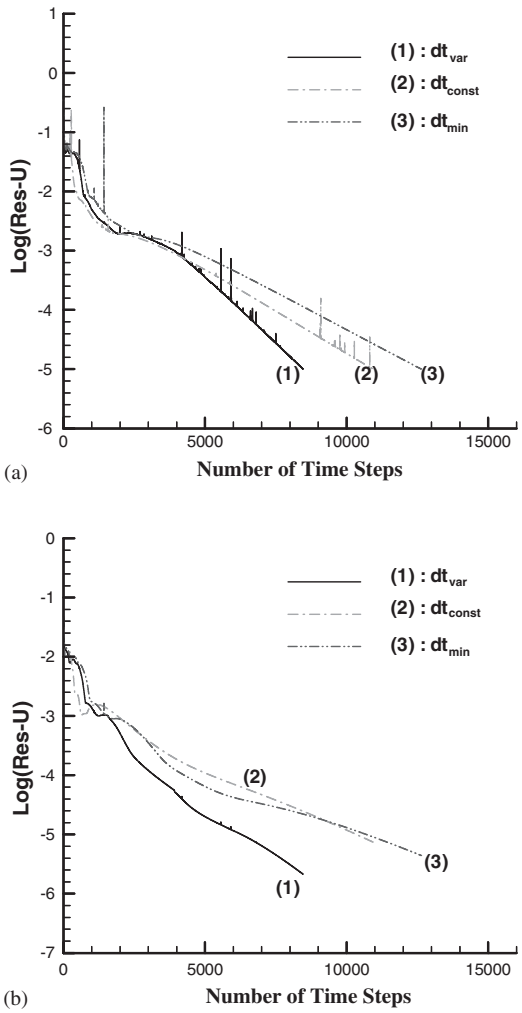

Figure 8. Residual histories for tested case 2 using Durbin's $k-\varepsilon-v^2$ model. (a) Velocity U; (b) turbulent kinetic energy.

due to the complexity of turbulence models and the high degree of flow complexity. The setting of stepsize of $(\Delta t)_{\max}$ also leads to quick divergence in test case 2 if Durbin's model is applied. The settings of time stepsize as $(\Delta t)_{\text{var}}$ and $(\Delta t)_{\text{const}}$ (Figure 8(a)) give a few irregular oscillations with a higher convergence rate for the axial velocity, but the setting of stepsize $(\Delta t)_{\min}$ provides a residual history without spikes and slowest convergence rate (Figure 8(b)). These computations indicate that the convergence is improved by the adoption of self-adjusted time stepsize for the complicated turbulence models and complex flow-fields, however, very small gain is obtained with severe oscillations and spikes if Lin's model is employed.

6. CONCLUSIONS

The determination of the time stepsize for each control volume and each time step is derived based on the concept of residuals minimization in the Bi-CGSTAB algorithm, and the self-adjusted stepsize concept in time span and spatial coordinate systems applied to improve convergence rate is proposed and tested for separated flow and advanced turbulence models. The flow-fields and temperature fields are computed numerically for the periodically turbulent flow or turbulent flow past a 2D-mounted rib using advanced turbulent models in low-Reynolds number forms as Launder–Sharma, Chien, Lin and Durbin's models. The convergence behaviors of computations demonstrate that this concept not only provides a guide of optimal determination of the time stepsize but also increases convergence rate for all advanced turbulence models tested.

REFERENCES

1. Hestens MR, Stiefel E. Methods of conjugate gradients for solving linear systems. *Journal of Research of the National Bureau of Standards* 1952; **49**:409–436.
2. Young DM, Jea KC. Generalized conjugate-gradient acceleration of non-symmetrizable iterative methods. *Linear Algebra and Its Applications* 1980; **34**:159–194.
3. Fletcher R. Conjugate gradient methods for indefinite systems. *Lecture Notes in Mathematics*, *Vol. 506*. Springer: Berlin, 1976; 73–89.
4. Sonneveld P. CGS, a fast Lanczos-type solver for nonsymmetric linear systems. *SIAM Journal on Scientific and Statistical Computation* 1989; **10**(1):36–52.
5. Van Der Vost. Bi-CGSTAB: A fast and smoothly converging variant of Bi-CG for the solution of non-symmetric linear systems. *SIAM Journal on Scientific and Statistical Computing* 1992; **13**(2):631–644.
6. Lin H, Yang DY, Chieng CC. Variants of Bi-conjugate method for compressible Navier–Stokes solver. *AIAA Journal* 1995; **33**(7):1177–1184.
7. Chuang CC, Chieng CC. Supersonic base-flow computation using higher order closure turbulence models. *AIAA Journal of Spacecraft and Rockets* 1996; **33**(3):374–380.
8. Smith GD. *Numerical Solution of Partial Differential Equations*: *Finite Difference Methods*. Oxford University Press: Oxford, 1986.
9. Strikwerda JC. *Finite Difference Schemes and Partial Differential Equations*. Wadsworth & Books/Cole Advanced Books & Software: Pacific Grove, California, 1989.
10. Pulliam TH. Artificial dissipation models for the Euler equations. *AIAA paper* 1985; 85-0438.
11. Saxena SK, Ravi K. Computation of three dimensional supersonic and hyperbolic blunt body flows using high order TVD scheme based on Roe's approximation Riemann solver. *Proceedings of the 14th International Conference on Numerical Methods in Fluid Dynamics*, Bangalore, India. *Lecture Notes in Physics* 1995; **453**: 520–524.
12. Arnone A, Pacciani R, Sesini A. Multigrid computations of unsteady rotor–stator intersection using the Navier–Stokes equation. *Journal of Fluids Engineering*, *Transaction of the ASME* 1995; **117**(4):647–652.
13. Mark A, Stephens T, Shih I-P. Flow and heat transfer in a smooth U-duct with and without rotation. *Journal of Propulsion and Power* 1999; **15**(2):272–279.
14. Soulis JV, Jovicic N, Milovanovic D, Babic M. Numerical modeling of incompressible turbulent flow in turbomachinery. '*98 European Computational Fluid Dynamics Conference*, 1998; 1, Issue Pr. 1:259–265.
15. Tsai WB, Lin WW, Chieng CC. Convergence acceleration by varying time stepsize using Bi-CGSTAB method for turbulent flow computation. *Numerical Methods in Partial Differential Equations 2001* (accepted for publication).
16. Archarya S, Dutta S, Myrum TA, Baker RS. The turbulent flow past a surface-mounted two-dimensional rib. *Transaction of the ASME*, *Journal of Fluids Engineering* 1994; **116**:238–246.
17. Archarya S, Dutta S, Myrum TA. Heat transfer in turbulent flow past a surface-mounted two-dimensional rib. *Transaction of the ASME*, *Journal of Heat Transfer* 1998; **120**:724–734.
18. Liou TM, Hwang JJ, Chen SH. Simulation and measurement of enhanced turbulent heat transfer in a channel with periodic ribs on one principal wall. *International Journal of Heat Mass Transfer* 1993; **36**(2):507–517.
19. Launder BE, Sharma BI. Application of the energy-dissipation model of turbulence to the calculation of flow near a spinning disc. *Letters in Heat and Mass Transfer* 1974; **1**:131–138.
20. Chien KY. Predictions of channel and boundary-layer flows with a low-Reynolds number turbulence model. *AIAA Journal* 1982; **20**(1):33–38.

21. Lin CA, Hwang CB. Improved low-Reynolds-number $k - \tilde{\varepsilon}$ model based on direct numerical simulation data. *AIAA Journal* 1998; **36**(1):38–43.
22. Durbin PA. Separated flow computations with the $k - \varepsilon - v^2$ model. *AIAA Journal* 1995; **33**(4):659–664.
23. Patankar SV. *Numerical Heat Transfer and Fluid Flow*. Hemisphere Publishing Corporation: Washington, 1980.

